PHILOSOPHICAL TRANSACTIONS OF THE ROYAL SOCIETY A MATHEMATICAL PHYSICAL & ENGINEERING SCIENCES

Dynamics of hazardous volcanic flows

Andrew W. Woodsy

Phil. Trans. R. Soc. Lond. A 2000 **358**, 1705-1724
doi: 10.1098/rsta.2000.0610

THE ROYAL SOCIETY

Dynamics of hazardous volcanic flows

By Andrew W. Woods†

Centre for Environmental and Geophysical Flows, University of Bristol, Bristol BS8 1TW, UK

In this paper, some of the processes involved in the generation and propagation of hazardous volcanic flows are described. The paper focuses on the high-speed dilute suspension flows that develop following

(i) the explosive collapse and decompression of a lava dome; and

(ii) the collapse of an ash-laden fountain erupting from a volcanic vent.

Using the model, we calculate the approximate vertical distribution of pressure in the flow, and show how this and the flow force evolve as the flow advances from the vent. The effects of topography and sedimentation on the intensity and run-out of such flows are described. Where possible, we draw on field examples of the different phenomena, and we review some analogue laboratory experiments that provide support for the modelling approach.

Keywords: ash flow; dynamics; hazards; explosion; sediment

1. Introduction

The dynamics of explosive volcanic flows has attracted considerable attention, owing to the devastating impact such flows may have on the terrain surrounding a volcano as well as the insights about the eruption conditions that may be deduced from the deposits (Druitt 1998). Numerous examples of high-energy volcanic flows have been recorded and studied over the past few decades. The massive explosive eruptions associated with the prehistoric eruption of Taupo, New Zealand (Wilson 1985), and the more recent flows at Mt Pinatubo in 1991 (Newhall & Punongbayan 1997) propagated tens of kilometres from the source at speeds of the order of 100 m s^{-1}. Collapse or failure of high-pressure lava domes can also lead to the formation of highly energetic flows of fine-grained particles and gas. Such flows occur on a smaller scale, but again propagate at speeds as large as many tens to 100 m s^{-1} (Fink & Kieffer 1993; Levine & Kieffer 1991). Important examples include the explosive flow activity at Mt Unzen Volcano, Japan, in 1991 (Sato *et al.* 1992), the dome collapse at the Soufrière Hills volcano, Montserrat, on 26 December 1997 (Sparks *et al.* 2000), and the explosive break up of the cryptodome at Mt St Helens on 18 May 1980 (Kieffer 1981). This latter event produced a lateral blast that travelled over 25 km from the volcano, causing immense destruction.

† Present address: BP Institute for Multiphase Flow, University of Cambridge, Madingley Rise, Cambridge CB3 0EZ, UK.

We now examine the dynamics of these dilute suspension flows produced by either the collapse of a pressurized lava dome or by the continuing flows associated with a more prolonged explosive eruption. We illustrate our discussion with reference to the 1980 eruptions of Mt St Helens, USA, and the recent eruptive activity of Soufrière Hills volcano, Montserrat. In § 2, we examine the dominant controls on the flow, and illustrate how the initial decompression-driven flow rapidly becomes dominated by the gravitational forces. We then develop a more detailed model of the main gravitationally driven part of the flow, and assess the sensitivity of the flow dynamics to the topography, grain-size distribution and basal friction. We also examine the role of sedimentation of particles from the bed as a function of position from the source. Our theoretical analysis is supported by experimental evidence from analogue laboratory experiments using particle-laden aqueous currents.

2. Dome collapse and decompression of high-pressure gas–particle mixtures

We now examine the decompression phase of the eruption, focusing on the explosive break-up of the dome. The main processes in such activity are sketched in figure 1 (after Woods *et al.* 2000). The intensity and scale of the blast flow may be estimated in terms of the energy released by the explosion. This energy is stored in the compressed gas, and has value (see, for example, Barenblatt 1996)

$$E \approx 2\pi\phi \int p(r) r^2 \, \mathrm{d}r, \tag{2.1}$$

where ϕ is the void fraction of the dome and $p(r)$ is the pressure at radius r in the dome. By assuming that the gas flows through the permeable dome according to Darcy's law, Woods *et al.* (2000) calculated that the internal dome pressure could be 1–2 orders of magnitude in excess of atmospheric pressure, in accord with independent theoretical calculations of the conduit ascent dynamics (Melnik & Sparks 2000). Woods *et al.* (2000) showed that such a pressure distribution in the dome can lead to very large values of the stored energy, in the range 10^{12}–10^{14} J, for typical conditions during the slow effusive growth of the dome prior to explosion (figure 2). This energy originates from the compressed gas and the fine-grained component of the solid material, which remains in thermal equilibrium with the gas during the explosion. This energy is able to drive the decompressing mixture away from the dome. Owing to the large mass of fine-grained material in equilibrium with the gas, the ratio of specific heats for the mixture of air and particles,

$$\frac{C_p}{C_v} = 1 + \frac{nR}{C_v}, \tag{2.2}$$

has a value very close to unity (Woods 1995). Therefore, the temperature of the mixture remains nearly constant as it is compressed or expands adiabatically. This may be understood to be a result of the thermal inertia of the solid material. We deduce that the pressure in the nearly isothermal, exploding mixture decays with distance at the approximate rate

$$p(r) \approx p(r_0)(r_0/r)^3. \tag{2.3}$$

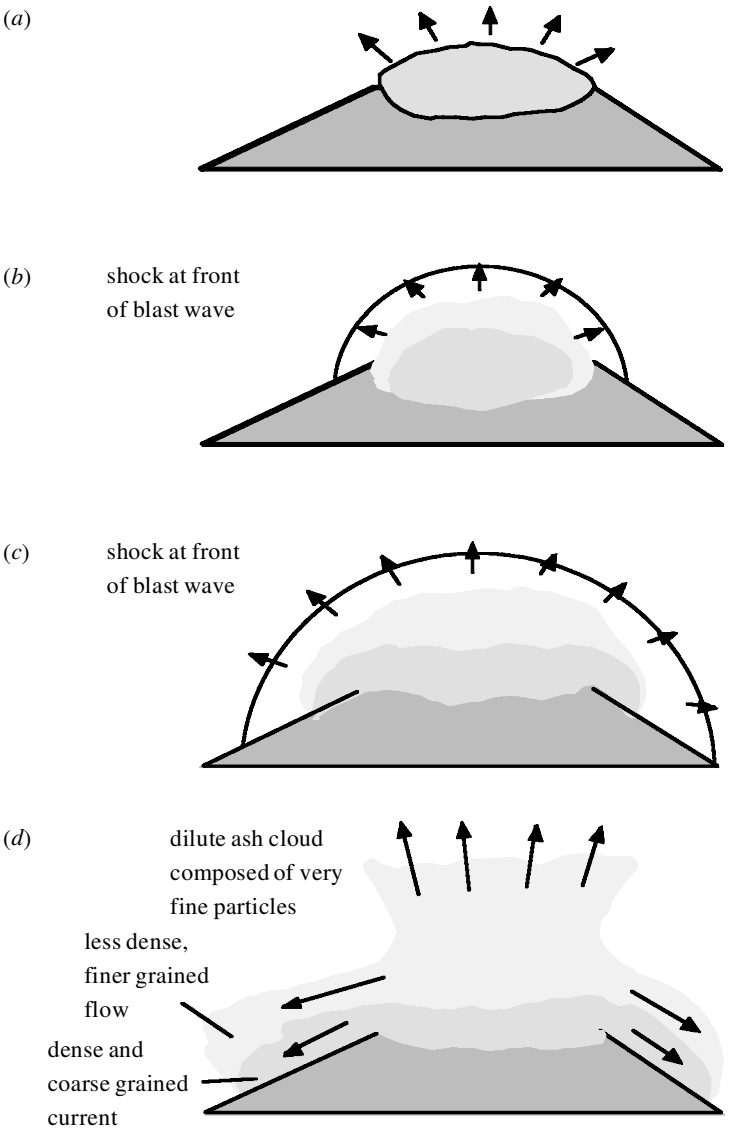

Figure 1. Schematic of the processes involved in the explosive decompression of a lava dome, including the initial break-up of the dome, the propagation of a blast wave with the concomitant dispersal of solid fragments, and, finally, the onset of the gravitationally controlled flow.

Numerical modelling of conduit flow suggests that pressurized domes may have initial pressures in the range 10^6–10^7 Pa within the void/pore spaces in the dome. This initial overpressure will fall below atmospheric within a distance of about 2–3 times the dome radius. For domes with radii of several hundred metres, this upper bound suggests that the initial overpressure will be dissipated within *ca.* 1 km of the dome. The subsequent motion will then gradually become dominated by the gravitational force acting on the relatively dense, particle-laden suspension. Taylor (1950) showed that for an instantaneous explosion, the position of the shock front, r_{f}, produced by

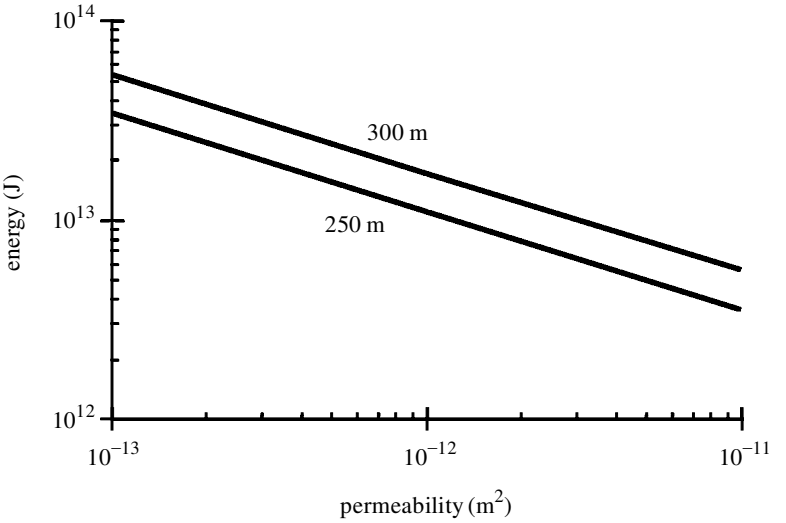

Figure 2. Energy stored as compressed gas in a steadily extruding dome of radius 250 and 300 m, assuming that the exsolved gas separates from the magma and percolates through the permeable dome material.

the sudden release of energy E is given by

$$r_{\mathrm{f}} = \left(\frac{Et^2}{\rho_0}\right)^{1/5}. \tag{2.4}$$

For the level of energy stored in the dome, such a blast wave would expand very rapidly with the material decompressing to atmospheric pressure within 0.5–5 s. This time-scale is likely to be considerably shorter than the time required for the break-up of the dome, and so we infer that the intensity of the initial flow may be limited by the rate of the break-up of the dome.

We now estimate the variation of the pressure with depth in the flow once the top of the flow has decompressed to atmospheric pressure. This calculation indicates that for deep flows, the gravitational force acting on the flow can produce pressures at the base of the flow that are in excess of atmospheric by an amount comparable with atmospheric pressure. First we consider the case of a sector of a dome that collapses to form a well-mixed dilute suspension of ash and gases in which the mass fraction of gas has value n. The flow will be well mixed if the mean speed of the flow exceeds the settling speed of the particles, so that particles remain suspended by the vertical turbulent motions in the flow (see, for example, Valentine 1987). Such mixing does not preclude the sedimentation of particles from the base of the flow. It is also important to comment that, although the particles remain suspended, if the flow is sufficiently deep, then the vertical gradient of flow pressure, associated with the weight of the flow, should lead to compression of the gas phase in the lower part of the flow. This can produce a vertical density gradient in the flow, as we illustrate below.

In a well-mixed suspension, the gas mass fraction, n, is independent of depth and

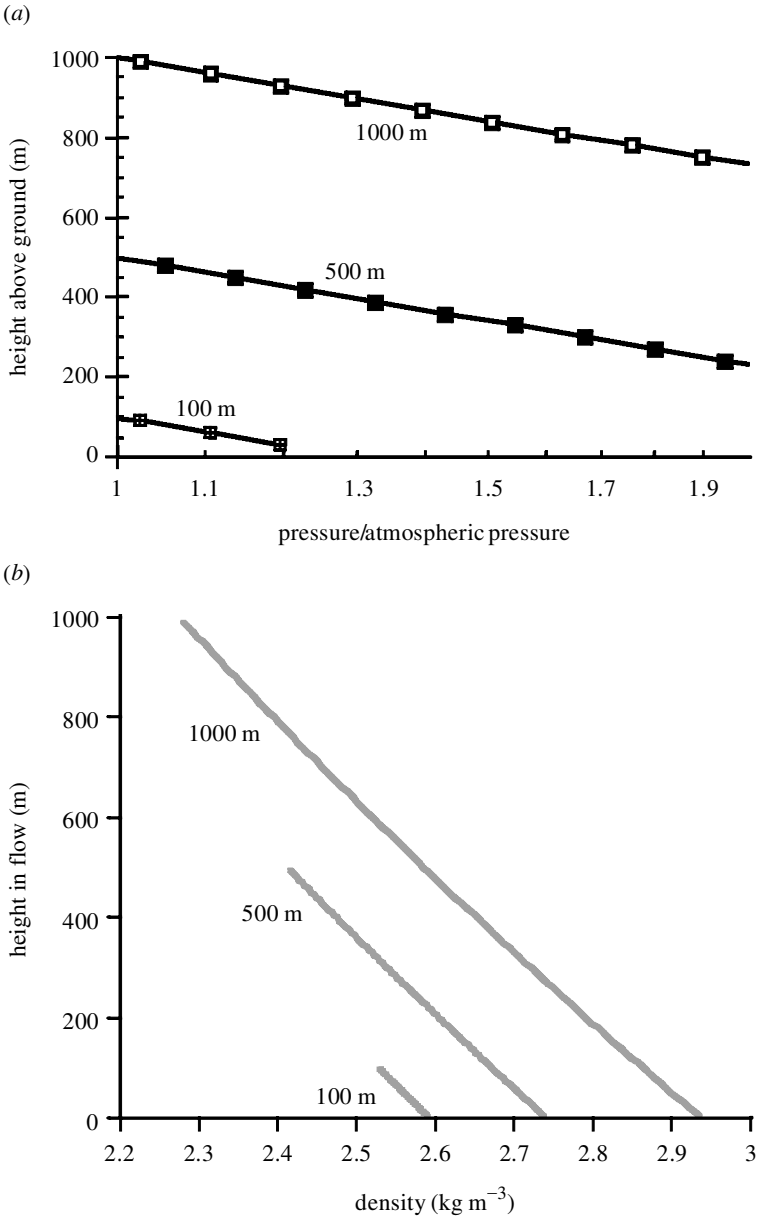

Figure 3. Vertical variation of (*a*) the pressure and (*b*) the density in the flow for a gas mass fraction of 0.1, a flow temperature 850 °C and gas constant 462 J kg^{-1} K^{-1}.

the local bulk density of the mixture is given by (see, for example, Woods 1995)

$$\rho = \left(\frac{nRT}{p} + \frac{1-n}{\rho_{\mathrm{s}}} \right)^{-1}, \tag{2.5}$$

where ρ_{s} is the solid density, and R and T are the gas constant and temperature,

respectively. For $R = 462\ \mathrm{J\,kg^{-1}\,K^{-1}}$, $p = 10^5$ Pa and $T = 850\ ^\circ\mathrm{C}$, it follows that

$$nRT\rho_s/p \gg 1 \tag{2.6}$$

whenever $n \gg 10^{-4}$. In this case, the density (2.5) may be approximated by the relation

$$\rho \approx p/(nRT). \tag{2.7}$$

As shown earlier, in equation (2.2), with a large mass fraction of fine-grained solid material, the temperature of the mixture is essentially constant, even if the turbulent motions are producing considerable vertical motion. Thus, the hydrostatic pressure varies with depth according to

$$\frac{\mathrm{d}p}{\mathrm{d}y} = -\frac{gp}{nRT}, \tag{2.8}$$

and so for a current of total depth h, the pressure at a point y (less than h) above the ground has value

$$p(y) = p(h)\exp\left(\frac{g(h-y)}{nRT}\right). \tag{2.9}$$

The gas mass fraction in the dilute flow depends on the mechanism of formation of the flow. The gas phase in a flow produced by a lateral blast may be similar to the original magmatic value, while that in a flow produced by a collapsing fountain may be considerably higher (cf. Bursik & Woods 1996). Here we take the value $n \sim 0.1$. In this case, the vertical scale over which the hydrostatic pressure in the flow changes by a factor e is of order 4 km, in contrast to the background atmospheric pressure, which evolves over a scale height of the order of 10 km (Gill 1981). Therefore, in ash flows that are several hundred metres deep, the internal hydrostatic pressure near the base of the flow may be significantly larger than atmospheric; this may be important in the context of damage that may be caused by the flow (figure 3*a*). For a flow with a gas mass of the order of 0.1, the density also varies with depth, ranging from about $2.3\ \mathrm{kg\,m^{-3}}$ at the upper surface to $2.9\ \mathrm{kg\,m^{-3}}$ in a 1000 m-deep flow (figure 3*b*). We deduce from this calculation that as the initial overpressure decays towards atmospheric, the hydrostatic pressure variations across the flow become increasingly significant. We will revisit this important point in § 3, where we consider the evolution of the flow pressure along the current.

3. The gravity-driven flow

We now build up a picture of the propagation of the pyroclastic density current generated by explosive fragmentation of the dome material. Our work builds on the progressive aggradation model of Branney & Kokelaar (1992), and the quantitative models of Bursik & Woods (1996) and Dade & Huppert (1996), although the model development is somewhat distinct. We introduce a number of approximations that allow us to simplify the model and develop some new analytic predictions to complement these earlier studies. We use the model of the flow evolution to evaluate the vertical variation in pressure along the flow path, and thereby estimate the possible impact of the flow on structures in the flow path.

We model the flow as a slowly evolving, gravity-driven flow that propagates along the ground, and in which the pressure on the upper surface of the current equals that of the overlying air. We examine the dynamics of a quasi-steady, two-dimensional flow, as might arise with a flow confined between the walls of a canyon. We obtain some approximate solutions for the structure of the flow as a function of distance from the source. This reveals much of the richness of the flow dynamics. We then turn to short-lived eruptions, in which the main part of the material is contained in the head of the flow. We introduce a simple scaling for the evolution of such flows, assuming that the conditions at the nose of the current are controlled by a quasi-steady force balance, as expressed by the so-called Froude-number condition. Finally, in § 4, we examine the analogous behaviour of radially symmetric flows.

(*a*) *Quasi-steady flow*

The flow dynamics are governed by equations for the conservation of mass and momentum. To leading order, in the absence of any entrainment of air, in a well-mixed flow the conservation of enthalpy is equivalent to the flow maintaining a constant temperature (Bursik & Woods 1996). The rate of entrainment of air into the flow depends on the Richardson number of the flow,

$$Ri = \frac{g\Delta\rho h}{\rho u^2},$$

with entrainment being important when Ri is small. In this limit, the kinetic energy in the flow exceeds the potential energy required to mix the relatively low density overlying air down into the flow. In a slow deep flow (subcritical regime), Ri is large and the entrainment is negligible, and it is this flow regime that we focus on herein. Supercritical flows, with $Ri < 1$, tend to entrain considerable quantities of air and have somewhat different dynamics (Bursik & Woods 1996); however, such flows are also unstable to hydraulic jumps in which they undergo a transition to subcritical flows.

We consider a flow advancing along a channel or canyon of fixed width. The mass flux of gas in the flow (per unit width), V, is maintained, although the solid mass flux (per unit width), S, may decrease owing to sedimentation,

$$V = \int_0^h \rho u n \,\mathrm{d}y, \tag{3.1}$$

$$\frac{\mathrm{d}S}{\mathrm{d}x} = \frac{\mathrm{d}}{\mathrm{d}x}\int_0^h \rho(1-n)u \,\mathrm{d}y \tag{3.2}$$

$$= -v_\mathrm{s}(1-n)\rho \quad (y=0), \tag{3.3}$$

where $1-n$ is the solid mass fraction and v_s represents the mean settling speed of particles in the current, which, for simplicity, we take as being constant (Bursik & Woods 1996). The sedimentation law (3.3) is a generalization of the settling law that has been introduced by various authors following Hazen (1904). Essentially, the law implies that particles that are swept to the base of the flow settle from the dilute suspension and into the basal deposit or some dense underflow. We assume that this simple settling law applies in the present complex flow, based on the successful application of the model to turbulent laboratory-scale flows (Bonnecaze *et al.* 1993;

Gladstone & Woods 2000). However, we note that there may be some additional effects owing to the structure of the turbulent boundary layer and the development of any dense undercurrent.

The momentum equation has the vector form

$$\rho \boldsymbol{u} \cdot \nabla \boldsymbol{u} = -\nabla p + \rho \boldsymbol{g} - f\rho \frac{|u|\boldsymbol{u}}{h}, \tag{3.4}$$

where the third term on the right-hand side represents the bottom drag acting on the flow. Since the flow is mainly parallel to the ground, and the length-scale over which the flow evolves is small compared with the flow depth, then the pressure is approximately hydrostatic. For a compressible flow, at height y above the ground, in a current of total depth h, the pressure has the value (§ 2)

$$p(x,y) = p_{\mathrm{a}}(x,h) \exp\left(\frac{g(h-y)}{n(x)RT}\right), \tag{3.5}$$

where p_{a} is the ambient pressure at height h above the ground. The integrated momentum equation in the direction of flow then reduces to the form

$$\frac{\mathrm{d}}{\mathrm{d}x}\int_0^H (\rho u^2 + p)\,\mathrm{d}y = -(1-n)v_{\mathrm{s}}\rho(x,0)\int_0^h \rho u\,\mathrm{d}y \Big/ \int_0^h \rho\,\mathrm{d}y, \tag{3.6}$$

where H is a constant such that $H > h$. Here, we have approximated the bottom drag as being negligibly small in comparison with the loss of momentum associated with the sedimenting material. This approximation is valid for relatively deep flows, $h >$ 10–100 m, with speed in the range 30–100 m s^{-1}, and with particles that sediment with speeds of the order of 1–10 m s^{-1}, if the value of the friction factor is in the typical range $f \approx 0.01$–0.001. The precise value of this empirical factor depends on the roughness scale of the terrain (Moody 1944). We also assume that the mass fraction of solid in the well-mixed current is independent of depth.

Bursik & Woods (1996) worked with the mean vertically averaged properties of the current and neglected the compressibility of the current. This is a good approximation if $hg \ll nRT$ and corresponds to a dilute or shallow current (less than 1000 m), containing a relatively large fraction of gas (greater than 0.1), in which the flow density is nearly uniform across the flow (figures 3 and 4). We adopt this approximation here to provide a leading-order description of shallow and dilute flows; later we use these solutions to approximate the detailed density and pressure profiles in the current, and, hence, to estimate the pressure anomalies associated with the dense flow. In this limit, the integral relations may be written

$$\frac{\mathrm{d}}{\mathrm{d}x}\left(\frac{u(1-n)h}{n}\right) = -\frac{(1-n)v_{\mathrm{s}}}{n}, \tag{3.7}$$

$$\frac{\mathrm{d}}{\mathrm{d}x}\left(h\left(\frac{u^2}{nRT} + \tfrac{1}{2}gh\left(\frac{1}{nRT} - \frac{1}{R_{\mathrm{a}}T_{\mathrm{a}}}\right)\right)\right) = -\frac{(1-n)v_{\mathrm{s}}u}{nRT}. \tag{3.8}$$

The second term on the left-hand side in equation (3.8) is associated with the potential energy of the flow. The model only applies while the flow is relatively dense, so that $nRT < R_{\mathrm{a}}T_{\mathrm{a}}$. We now develop some solutions for the motion of ash flows that

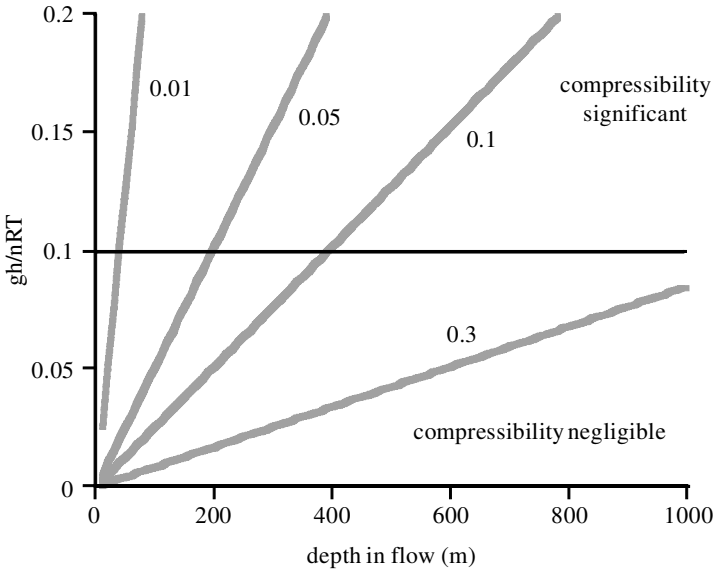

Figure 4. Diagram showing contours of hg/nRT as a function of the flow depth h for several values of the gas mass fraction n to establish conditions under which the simple well-mixed model applies and the effects of compressibility are negligible.

are valid in this limit of essentially incompressible flow, as described by (3.7) and (3.8). In this limit, the conservation of gas requires that

$$uh = V_{\mathrm{g}}, \tag{3.9}$$

where V_{g} is the gas volume flux (per unit width cross-flow). Then combining equations (3.7)–(3.9) leads to the expression for the rate of change of the gas mass fraction in the flow

$$n = \left(1 + \frac{1-n_0}{n_0}\exp\left(\frac{-v_{\mathrm{s}}x}{V_{\mathrm{g}}}\right)\right)^{-1}, \tag{3.10}$$

and to the momentum conservation relation (cf. (3.8))

$$\frac{\mathrm{d}}{\mathrm{d}x}\left(\frac{u}{n} + \frac{gV_{\mathrm{g}}}{2u^2n}\left(1 - \frac{nRT}{R_{\mathrm{a}}T_{\mathrm{a}}}\right)\right) = -\frac{(1-n)}{n}\frac{v_{\mathrm{s}}u}{V_{\mathrm{g}}}. \tag{3.11}$$

Equation (3.11) identifies that the critical velocity scales as

$$(1-\lambda n)^{1/3}(gV_{\mathrm{g}})^{1/3},$$

and that the sedimentation length of the current is $V_{\mathrm{g}}/v_{\mathrm{s}}$, leading to the dimensionless equation

$$\frac{\mathrm{d}}{\mathrm{d}X}\left(\frac{1}{n}\left(U + \frac{(1-\lambda n)}{2U^2}\right)\right) = -\frac{(1-n_0)}{n_0}\exp(-X)U, \tag{3.12}$$

where the scaled variables are given by

$$\lambda = \frac{RT}{R_{\mathrm{a}}T_{\mathrm{a}}}, \quad U = (gV_{\mathrm{g}})^{1/3}u \quad \text{and} \quad X = \frac{xv_{\mathrm{s}}}{V_{\mathrm{g}}}. \tag{3.13}$$

The top of the current becomes neutrally buoyant when the gas content has increased to the value

$$n = 1/\lambda, \tag{3.14}$$

and this coincides with the point

$$x = -\frac{V_g}{v_s} \log\left(\frac{n_0(\lambda - 1)}{1 - n_0}\right). \tag{3.15}$$

The above model of an incompressible flow captures the key controls on the motion of a turbulent ash, and is valid for flows of the order of a few hundred metres deep or shallower, with flow speeds in excess of the fall speed of the particles. This approximation is especially relevant for radially spreading flows, which become progressively shallower with distance from the source (§ 4). Typical particles of size 0.01–1.0 cm have fall speeds in the range 0.1–10 m s^{-1}. The model may be used to examine some of the hazards associated with ash flows, and, in particular, to estimate the pressure forces that may be exerted on buildings in the path of the flow. We now develop some numerical solutions to the equations (3.7)–(3.9).

The calculations of figure 5 identify the evolution of (a) the velocity, and (b) the gas mass fraction with distance in the flow as predicted by the model. Figure 5*a* shows that subcritical flows, which move with speeds smaller than the critical speed of the flow (i.e. the speed of gravity waves associated with the dense particle-laden flow), tend to decelerate and deepen as they sediment, while supercritical flows accelerate and thin. We therefore expect that the hydrostatic pressure associated with subcritical flows will remain quite elevated at the base of the flow, even though the flow is sedimenting, and this may have an important impact on building damage caused by the flow. As mentioned above, supercritical flows are likely to entrain air, thereby increasing their mass. This increases the rate at which they become buoyant (Bursik & Woods 1996). In the present work, we focus on subcritical flows.

Figure 5*b* illustrates how the gas mass fraction in the flow progressively increases through sedimentation. When the flow has sedimented a sufficient mass of material and the gas mass fraction has become sufficiently large, then the residual flow will become less dense than the surrounding air. At this stage, the flow will lift off. In practice, since the flow does have a vertical density structure, the uppermost material first becomes less dense than the surrounding ambient. As this lifts off, and the sedimentation proceeds, then the interior fluid in the current will become progressively less dense than the surrounding air. The lift-off process will then occur over a finite distance, rather than being instantaneous. This is because as the buoyant material in the upper part of the flow separates from the main body of the flow, further sedimentation may be needed for material located progressively deeper in the flow to become buoyant. However, the present approximate model enables us to estimate the initial point of buoyant lift-off for material at the top of the flow. Indeed, figure 6 illustrates how the run-out distance predicted by equation (3.15) rapidly decreases with the initial gas mass fraction in the flow, assuming a particular volume flux and settling speed of the particles. The calculations also illustrate the influence of the flow temperature: cold flows propagate further, as they are less buoyant than their hotter counterparts and need to sediment more material before lifting off.

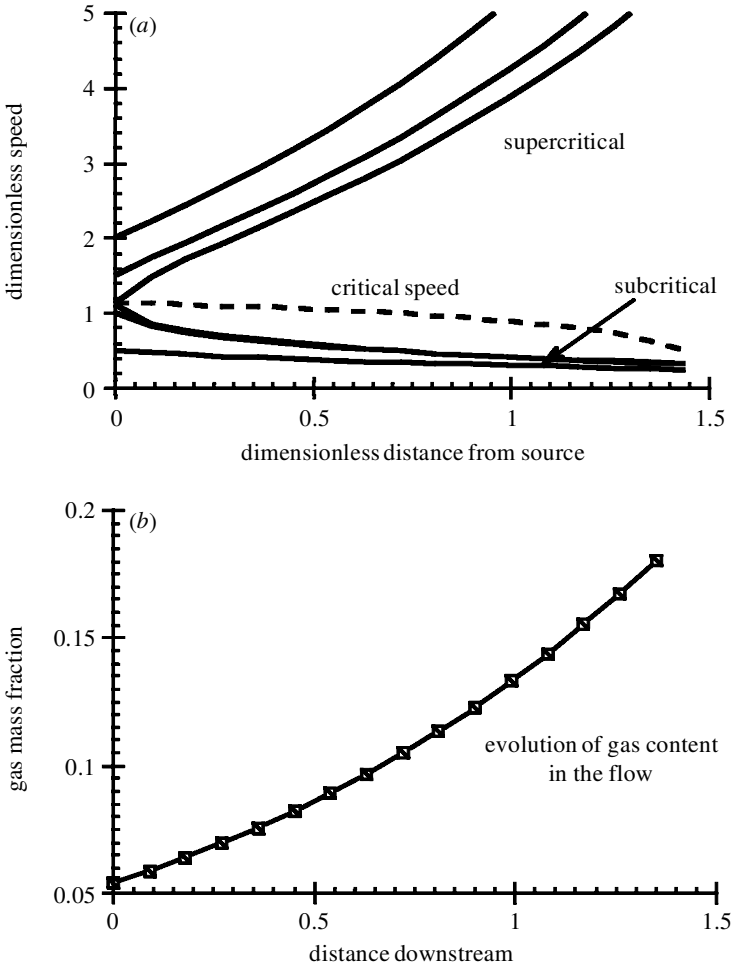

Figure 5. Illustration of the evolution of the flow speed (a) and the gas mass fraction (b) with distance from the source for a steady flow. In (a), the different curves correspond to different initial flow speeds. The subcritical profiles identify how the velocity falls off, with an associated deepening of the flow. For the cases shown, the flow only propagates about 1.5 times the e-folding scale for the sedimentation before the mixture becomes buoyant.

Since the flows tend to sediment and evolve as they propagate, the vertical pressure gradient within the flow, and the flow depth, changes with position. In figure 7 we illustrate the fractional difference between the flow pressure and atmospheric pressure as a function of height in the current for three distances downstream of the source. The calculations have been made for a typical subcritical flow. In the figure, the difference between the flow pressure and the ambient pressure increases with depth below the top surface of the flow. The maximum pressure of the flow arises at the base. This maximum pressure decreases with distance from the source even though the flow deepens as it moves, because the particle load of the flow decreases through sedimentation. In this calculation, it may be seen that the pressure may take values as much as 20–30 kPa above atmospheric pressure. These results are also sensitive

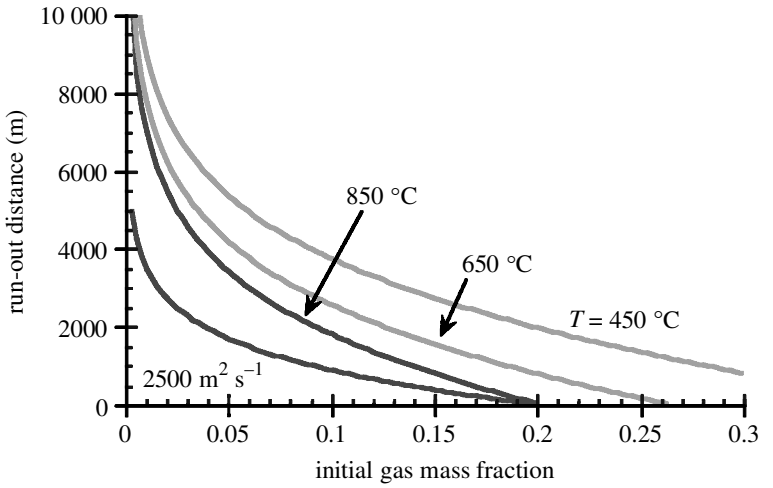

Figure 6. Variation of the run-out distance with initial gas content, and initial temperature of the flow. The calculations are based on a subcritical flow with a flux of 5000 m^2 s^{-1}.

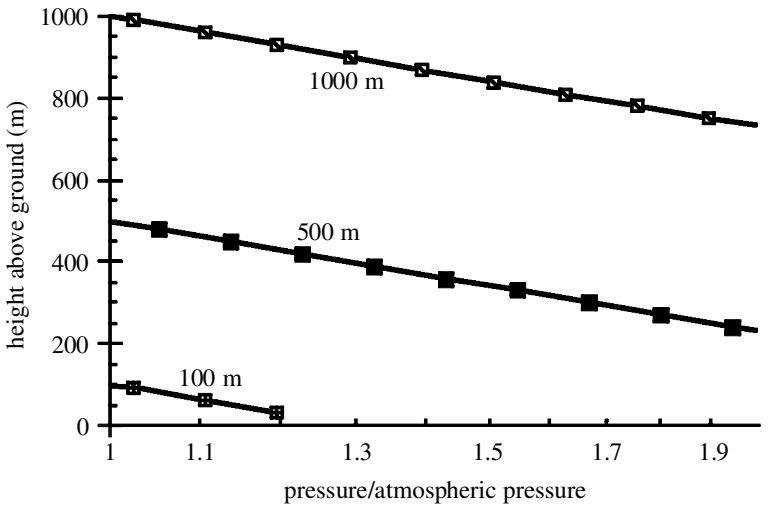

Figure 7. Variation of the pressure with depth in flow. Note that the pressure variation is approximately linear with height, since, for such shallow currents, the flow density is nearly uniform with height. This calculation is based on a gas mass fraction of 0.1.

to the initial gas content of the flow. In this calculation, we take the gas content to be 0.1 by mass. Based on evidence of pressure damage from nuclear explosions, such pressures may cause significant damage to a building (Valentine 1998). However, the nature of the damage may be rather different in that, in addition to the excess hydrostatic pressure, the building is bombarded by a highly particulate fast flow. This leads to an erosive flow and dynamic pressure that arises as the momentum of the oncoming flow is arrested and redirected.

If we neglect the effects of boundary layers, and also assume that the pressure on the downstream side of the wall remains at atmospheric pressure, then we can

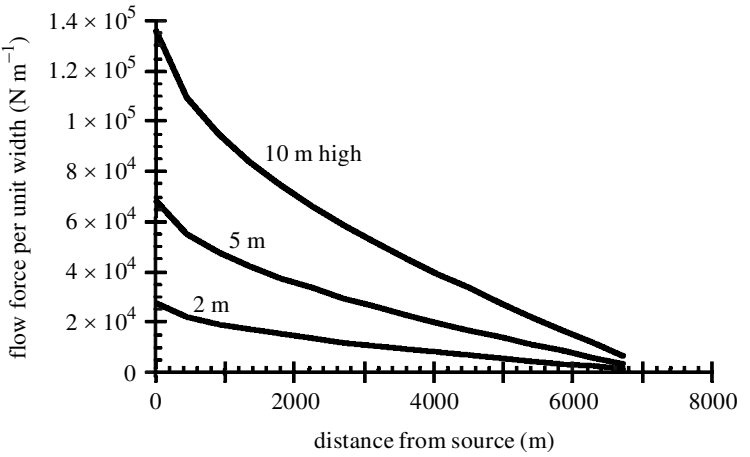

Figure 8. Variation of the flow force with the downstream position in the current, for a two-dimensional channelled flow. The calculations are based on a subcritical flow with a flux of 5000 $\mathrm{m}^2\ \mathrm{s}^{-1}$ (figure 5).

calculate the net force exerted by a relatively shallow flow of depth h, on a wall of height $H > h$. We assume that force exerted by the wall on the flow diverts the flow around the wall; this force is given by the combination of hydrostatic and dynamic pressures, as may be calculated from the momentum equation, giving the total flow force:

$$F = \frac{Vp(0)}{nRT}\left(u + \frac{gh}{2u}\left(1 - \frac{nRT}{R_{\mathrm{a}}T_{\mathrm{a}}}\right)\right). \tag{3.16}$$

However, most flows are in fact sufficiently dilute that they are deeper than the obstacles in their path. The flow force on an obstacle that is of height $H < h$, and which is located on the ground, is given by integration of the momentum equation from the ground to height H. Again, examining the initial stage of this flow, in which the pressure on the downstream side of the wall will have the smaller atmospheric value, so that both the hydrostatic and dynamic pressures contribute to the force, we find that the flow force is

$$F = \left(\frac{H}{h}\right)\frac{Vp(0)}{nRT}\left(u + \frac{g(2h - H)}{2u}\left(1 - \frac{nRT}{R_{\mathrm{a}}T_{\mathrm{a}}}\right)\right). \tag{3.17}$$

In figure 8 we illustrate how the flow force evolves with distance downstream for obstacles of height $H = 10$ m, 5 m and 2 m in a flow of magnitude $10^6\ \mathrm{kg\,s^{-1}\,m^{-1}}$. Note that if the obstacle lies in the lower boundary layer of the flow, then the velocity will be smaller than predicted herein, and so the present estimate of the flow force should be regarded as an upper bound. Furthermore, as the flow passes around the obstacle and the downstream hydrostatic pressure adjusts to that of the flow, then the hydrostatic component of the force will become smaller, and the main force on the wall will be associated with the change in momentum as the flow is diverted around the wall.

In deeper flows, the variation of the flow density and pressure with depth may be considerable (figure 3). In such flows, the approximation of a uniform velocity

and density, independent of depth, may be less appropriate, and the flow dynamics becomes more complex. Shear may develop in the mean-flow profile. Such effects may be very important near the source, and could lead to some lateral segregation of the flow. However, in many cases, the flow tends to spread radially from the vent, and will, therefore, rapidly thin out, reducing the flow depth and the associated large hydrostatic pressures. In § 4 we briefly extend the modelling to the case of radial flows, to examine the evolution of the flow including the geometrical spreading of the current.

(*b*) *Short-lived flows*

In a flow of short duration, the main mass of the flow may be contained in the leading head of the flow rather than in the main body of the flow that follows. This may have been the case during the eruption of Mt Pelée, Martinique in 1902 (Lacroix 1904), and the prehistoric eruption of Taupo volcano, New Zealand (Dade & Huppert 1996). In this situation, the flow may be modelled using the same density relation as described above (equation (2.6)), but the flow dynamics is simplified with a so-called Froude-number condition for the speed of the head of the flow, that is

$$u = Fr(gh(1-\lambda n))^{1/2}. \tag{3.18}$$

This relation is similar to the critical velocity of the current described in the previous section. The relation is coupled with the global conservation of mass, which has the form

$$V_{\mathrm{g}} = hL, \tag{3.19}$$

where V_{g} is the volume of gas per unit width, h and L are the averaged depth and lateral extent of the current, and Fr is the Froude number of the current, with a typical value of 1.2 (Simpson 1997). Also, the particles sediment from the flow at a rate given by

$$\frac{\mathrm{d}n}{\mathrm{d}L} = \frac{v_{\mathrm{s}} n(1-n)L}{V_{\mathrm{g}} u}. \tag{3.20}$$

Coupling these results, we can deduce the relation between the gas content of the flow and the run-out length

$$L^{5/2} = L_0^{5/2} + \frac{5V_{\mathrm{g}}^{3/2} g^{1/2} Fr}{2v_{\mathrm{s}}} \int_{n_0}^{n} \frac{(1-\lambda n)^{1/2}}{n(1-n)}\,\mathrm{d}n, \tag{3.21}$$

where L_0 and n_0 are the initial length and gas content of the flow. This specifies how the gas content of the flow varies with the distance propagated by the nose. Using the definition of the speed of the flow, $u = \mathrm{d}L/\mathrm{d}t$, we can then solve the system to determine the particle load and position of the nose of the current as a function of time. Figure 9*a* illustrates the typical run-out distance as a function of the initial volume of the cloud and the mean settling speed of the particles.

(*c*) *Experimental tests of modelling approach*

The theoretical approach to modelling ash flows described herein has been successfully tested using a series of analogue particle laden laboratory currents (Bonnecaze

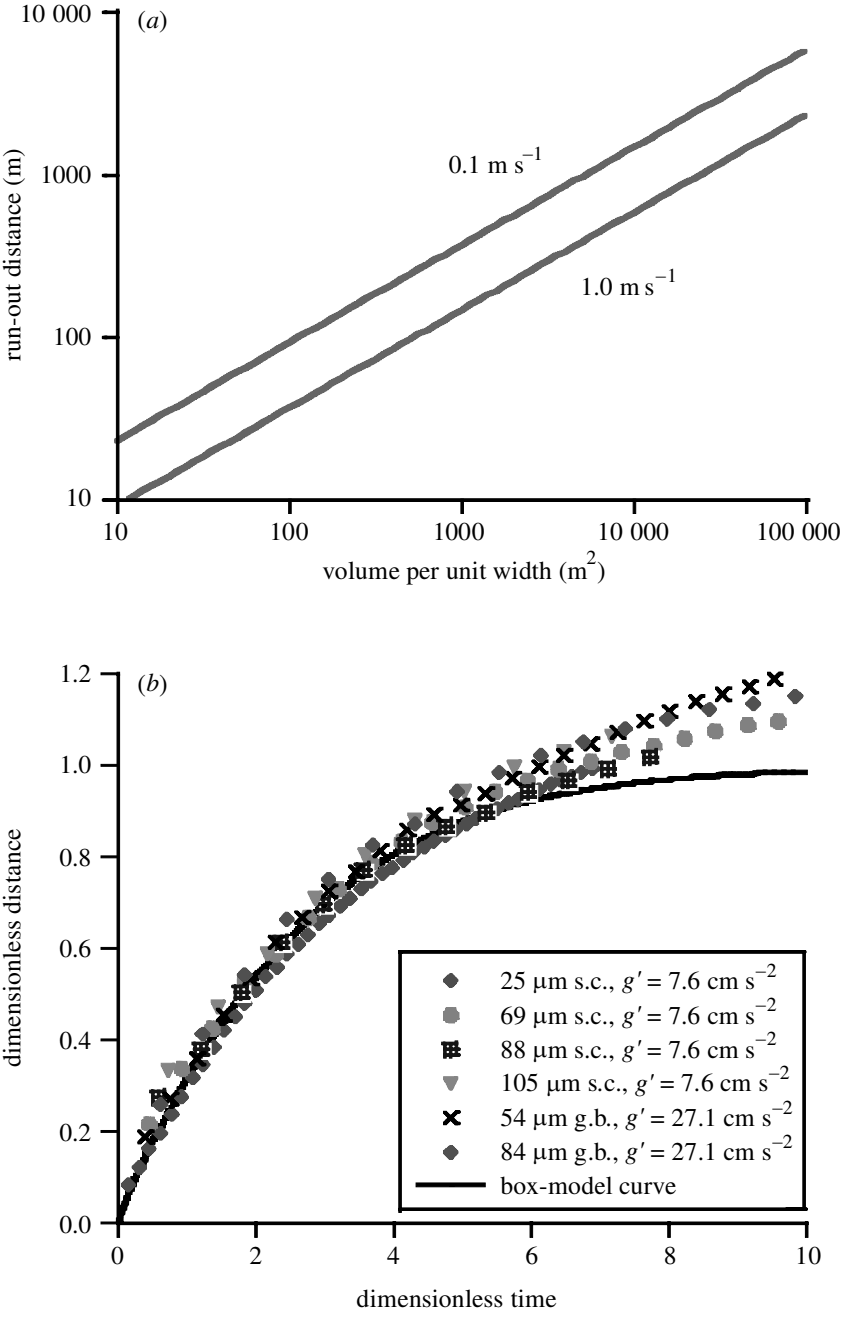

Figure 9. (*a*) Run-out distance of a theoretical ash flow produced from a short-lived eruption and discharging into a channel of fixed width. Numbers on curves show mean fall speed of particles. (*b*) Position of a particle-laden gravity current as a function of time, comparing experimental measurements with theoretical prediction. The data are dimensionless, so that a series of different experiments are compared with the universal dimensionless prediction of the model (after Gladstone & Woods (2000)).

et al. 1993; Woods *et al*. 1998; Gladstone & Woods 2000). These experiments are designed to be dynamically similar to the high-Reynolds-number flow regime that applies to large turbulent ash flows (see, for example, Woods *et al*. 1998). In the analogue laboratory experiments, particle laden volumes of fresh water are released from behind a lock gate into a flume filled with fresh water. The position of the head of the particle-laden current as it advances down a flume is then measured as a function of time. The model of § 3 *b* was adapted for application to the laboratory situation—primarily by use of the Boussinesq approximation, i.e. that the density contrast between the advancing current and the ambient fluid is small—and only needs to be accounted for in the definition of the flow speed, which depends on the density contrast between the fluids (cf. equation (3.18)). In figure 9*b*, we compare the predictions of the model with a series of experimental measurements of currents for various particle sizes with different fall speeds (after Gladstone & Woods 2000); the good agreement illustrates the power of such simple modelling.

4. Radial flows

The analysis described in § 3 *a* may be extended to the case of radial flow, by modelling the flow through a series of cylindrical annuli centred at the source. Extension of the model then leads to a series of revised conservation laws for flow across cylindrical surfaces centred at the source. The volume flux of gas is given by the quantity

$$Q = 2\pi r u h, \tag{4.1}$$

while the mass fraction of gas in the flow evolves according to the modified relation

$$n(R) = \left(1 + \frac{1 - n(0)}{n(0)} \exp(-\tfrac{1}{2}R^2)\right)^{-1}. \tag{4.2}$$

Finally, the momentum equation simplifies to the form

$$\frac{\mathrm{d}}{\mathrm{d}R}\left(\frac{1}{n}\left(U + \frac{(1-\lambda n)}{2U^2 R}\right)\right) = -\frac{(1-n(0))}{n(0)} \exp(-\tfrac{1}{2}R^2) U R, \tag{4.3}$$

in terms of the dimensionless velocity U and radius R, where the velocity scales according to the relation

$$U = \frac{(2\pi)^{1/6} u}{(g^2 Q v_\mathrm{s})^{1/6}}, \tag{4.4}$$

and the radius scales with the length-scale of sedimentation from the flow, as given by the relation

$$R = \left(\frac{2\pi v_\mathrm{s}}{Q}\right)^{1/2} r. \tag{4.5}$$

The evolution of these flows is somewhat different owing to the radial spreading of the flow (see, for example, Bursik & Woods 1996). However, the subcritical flow again exhibits similar characteristics, deepening and slowing as the flow evolves.

The radial location of the point where the flow density falls to that of the environment is now given by

$$r = \left(-\frac{Q}{2\pi v_\mathrm{s}} \log\left(\frac{n(0)(\lambda - 1)}{1 - n(0)}\right)\right)^{1/2}. \tag{4.6}$$

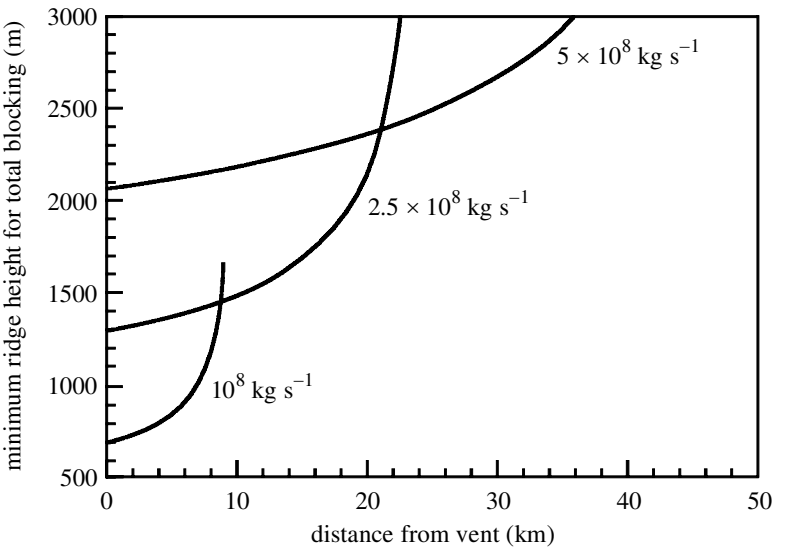

Figure 10. Maximum height of obstacle of slowly varying depth that a steady two-dimensional flow may scale as a function of distance from the source (after Woods *et al.* (1998)). Curves are shown for different eruption rates in a 2 km wide channel.

5. Topography and density stratification

The modelling we have described indicates some of the key properties of dilute suspension flows of hot gas and particles, and, in particular, how the flow density and pressure evolve with distance downstream. However, there are some important additional constraints on the flow that may lead to a richer, more-complex evolution of the flow. We examine two important effects below.

(*a*) *The interaction with topography*

First, we briefly examine the interaction of the flow with topographical obstacles such as ridges, and we assess the ability of the flow to scale such barriers as a function of distance from the source. Our analysis is based on that presented by Woods *et al.* (1998). Essentially, we consider the flow on the local scale of a topographic obstacle to the flow, and assume that for a sufficiently large flow there is negligible sedimentation during this process. As the flow scales the obstacle, the distribution of kinetic and potential energies may be exchanged, in accord with the usual results from channel hydraulics. Therefore, as the flow spreads further from the source, and the flow density decreases through sedimentation, the height of obstacle that the flow may scale increases (figure 10). Indeed, eventually the flow will lift off.

(*b*) *Density stratification and analogue laboratory models*

In the models described in this paper, we have assumed that the flows are well mixed, with the mass fraction of particles remaining independent of depth. This may not always be the case. Indeed, during both the initial decompression phase (Woods *et al.* 2000) and the subsequent motion, as the flow decelerates, the coarsest

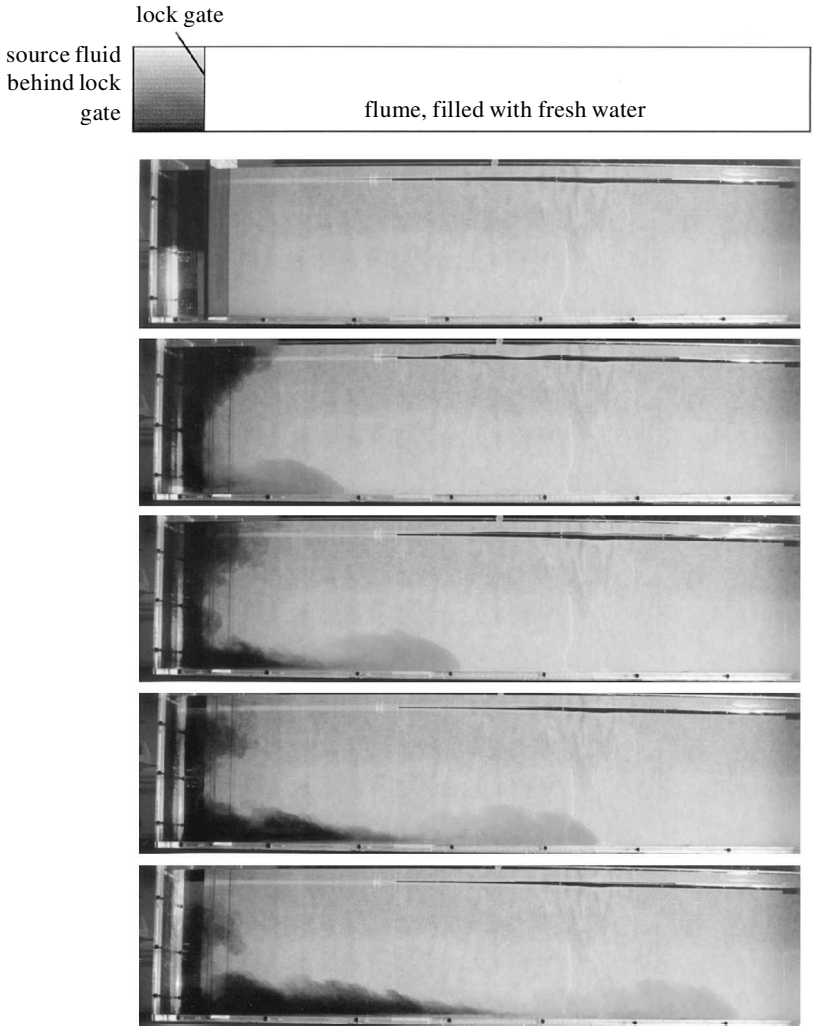

Figure 11. Evolution of a two-layer gravity current in which the upper layer has a buoyancy one-quarter of the value of the lower layer (after Woods *et al.* (2000)). The lower dense layer runs ahead, and the flow appears to separate laterally as it evolves down the flume.

particles settle towards the base of the flow. This can lead to vertical stratification of the particle loading in the flow (Valentine 1987). Although the dynamics of such stratified gravity currents is complex and relatively unexplored, a number of recent experiments have cast some light on their dynamics (Woods *et al.* 2000). One of the key new findings is that with a density-stratified source, the lower dense part of the flow may run ahead of the overlying less dense fluid, depending on the density contrast and structure of the stratification. As shown in the experimental sequence in figure 11, this may lead to more-ordered sedimentation patterns and a different flow morphology in contrast with the simplified picture of a well-mixed flow; this will form the subject of future research.

6. Summary and discussion

In this contribution, we have described some aspects of the process by which a high-pressure dome fails and decompresses, thereby producing a dilute gravity-driven suspension flow, often known as a surge flow. The dynamics of such surges have been examined using a series of simplified models for both quasi-steady and instantaneous eruption of material; the instantaneous model describes the advance of the head of the flow, while the quasi-steady model applies to the continuing flow of material that may arise if the conduit is opened by the collapse. The modelling has identified that the sedimentation of particles from the flow has a key impact on the density evolution, and, hence, the flow dynamics. The run-out distance decreases as either the sedimentation velocity or the initial gas content of the erupting material increases, or as the mass eruption rate decreases. The modelling has also identified that, even for small flows, the excess pressure in the flow, in addition to the background atmospheric pressure, may be very significant, even in flows of a quite modest scale. Calculation of the flow force acting on an obstacle impacted by the flow confirm observations that the flow may impart significant damage to buildings. This damage may arise from both the initial impact of the flow, when the hydrostatic pressure in the flow exceeds that in the ambient fluid surrounding the obstacle, but also during the continuing flow, owing to the change in momentum of the flow as it is redirected around the obstacle. Finally, we have described some complexities that might develop in ash flows if there is any initial stratification of the particles in the flow, or as flows interact with obstacles.

I have benefited from discussions with many colleagues, including Steve Sparks, Claude Jaupart, Marcus Bursik and Andrew Hogg, about the work herein and related problems. I also thank Lucy Richie and Charlotte Gladstone for figure 11 from Woods *et al.* (2000).

References

Barenblatt, G. 1996 *Scaling, self-similarity and intermediate asymptotics.* Cambridge University Press.

Bonnecaze, R., Lister, J. & Huppert, H. 1993 Particle laden gravity currents. *J. Fluid Mech.* **250**, 339–369.

Branney, M. & Kokelaar, P. 1992 A reappraisal of ignimbrite emplacement: progressive aggradation and changes from particulate to non-particulate flow during emplacement of high grade ignimbrite. *Bull. Volc.* **54**, 504–520.

Bursik, M. & Woods, A. W. 1996 The dynamics and thermodynamics of ash flows. *Bull. Volc.* **58**, 175–193.

Dade, B. & Huppert, H. 1996 Emplacement of the Taupo ignimbrite by adilute turbulent flow. *Nature* **381**, 509–512.

Druitt, T. 1998 Pyroclastic density currents. In *The physics of explosive volcanic eruptions* (ed. J. Gilbert & R. S. J. Sparks). Geological Society of London (Spec. Publ.) **145**, pp. 145–182.

Fink, J. & Kieffer, S. 1993 Estimates of pyroclastic flow velocities from explosive decompression of lava domes. *Nature* **363**, 612–615.

Gill, A. E. 1981 *Atmosphere–ocean dynmaics.* Academic.

Gladstone, C. & Woods, A. W. 2000 An experimental test of box models for particle laden gravity currents. *J. Fluid Mech.* (In the press.)

Hazen, A. 1904 On sedimentation. *Trans. Am. Civ. Engng* **3**, 45–88.

Kieffer, S. 1981 Fluid dynamics of the May 18 blast at Mount St Helens. In *The 1980 eruptions of Mount St Helens* (ed. P. Lipman & D. R. Mullineaux). *US Geol. Surv. Prof. Paper* **1250**, 545–570.

Lacroix, A. 1904 *La Montagne Pelée and its eruptions*. Paris: Masson & Cie.

Levine, A. & Keiffer, S. 1991 Hydraulics of the August 7 1980 pyroclastic flow at Mount St Helens, Washington. *Geology* **19**, 1121–1124.

Melnik, O. & Sparks, R. S. J. 2000 Dynamics of lava ascent and magma extrusion at Soufrière Hills volcano, Montserrat. Geological Society of London (Spec. Publ.). (Submitted.)

Moody, L. F. 1944 Friction factors for pipe flows. *Trans. ASME* **66**, 671.

Newhall, C. & Punongbayan, R. S. 1997 *Fire and mud: eruptions and lahars of Mount Pinatubo, Philippines*. Seattle, WA: University of Washington Press.

Sato, H., Fujii, T. & Nakada, S. 1992 Crumbling of dacite lava and generation of pyroclastic flows at Unzen volcano. *Nature* **360**, 664–666.

Simpson, J. 1997 *Gravity currents*. Cambridge University Press.

Sparks, R. S. J. (and 11 others) 2000 Generation of a debris avalanche and violent pyroclastic density current: the Boxing day eruption of 26th December 1997, Soufrière Hills, Montserrat. Geological Society of London (Spec. Publ.). (In the press.)

Taylor, G. I. 1950 The formation of a blast wave by an intense explosion. *Proc. R. Soc. Lond.* A **201**, 159–186.

Valentine, G. 1987 Stratified flow in pyroclastic surges. *Bull. Volc.* **49**, 616–630.

Valentine, G. 1998 Damage to structures by pyroclastic flows and surges inferred from nuclear weapons effects. *J. Volc. Geotherm. Res.* **87**, 117–140.

Wilson, C. J. N. 1985 The Taupo eruption, New Zealand. II. The Taupo ignimbrite. *Phil. Trans. R. Soc. Lond.* A **314**, 229–310.

Woods, A. W. 1995 The dynamics of explosive volcanic eruptions. *Rev. Geophys.* **33**, 495–530.

Woods, A. W., Bursik, M. I. & Kurbatov, A. 1998 The interaction of ash flows with ridges. *Bull. Volc.* **60**, 38–51.

Woods, A. W., Sparks, R. S. J., Batey, J., Gladstone, C., Ritchie, L. & Bursik, M. 2000 The generation of stratified surge deposits generated from explosive dome collapse. The December 26 1997 eruption of Soufrière Hills volcano, Montserrat. Geological Society of London (Spec. Publ.). (Submitted.)

PHILOSOPHICAL TRANSACTIONS OF THE ROYAL SOCIETY A MATHEMATICAL, PHYSICAL & ENGINEERING SCIENCES